Langmuir

ARTICLE

pubs.acs.org/Langmuir

On Modulating the Self-Assembly Behaviors of Poly(styrene-*b*-4-vinylpyridine)/Octyl Gallate Blends in Solution State via Hydrogen Bonding from Different Common Solvents

Shih-Chien Chen,[†] Shiao-Wei Kuo,[‡,*] and Feng-Chih Chang[†,*]

[†]Institute of Applied Chemistry, National Chiao Tung University, Hsin Chu, 300 Taiwan

[‡]Department of Materials and Optoelectronic Science, Center for Nanoscience and Nanotechnology, National Sun Yat-Sen University, Kaohsiung, 804, Taiwan

Supporting Information

ABSTRACT:

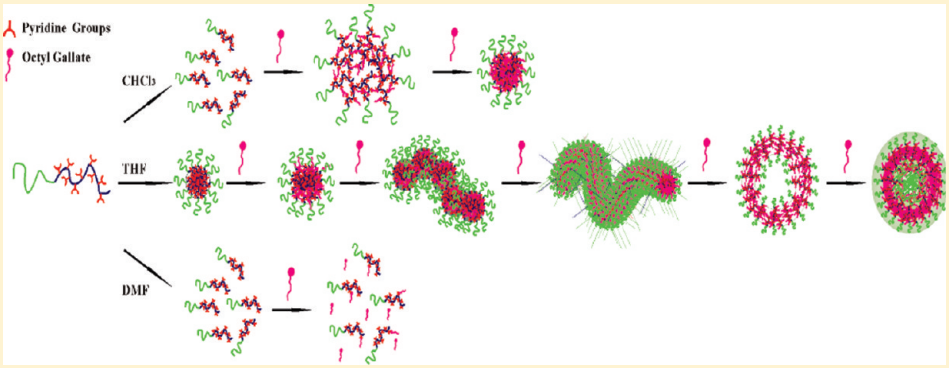

We have investigated the complexation-induced phase behavior of the mixtures of poly(styrene-*b*-4-vinylpyridine) (PS-*b*-P4VP) and octyl gallate (OG) due to hydrogen bonding in different solvents. The Fourier transform infrared spectroscopic result indicates that the hydrogen-bonding was formed between the P4VP blocks and OG in both THF and DMF, implying the P4VP blocks can bind to OG. For PS-*b*-P4VP/OG mixture in chloroform, the morphological transitions were induced from the unimer configuration to swollen aggregate and complex-micelles by adding OG. Interestingly, the complex-micelles can lead the formation of the honeycomb structure from chloroform solution. The PS-*b*-P4VP/OG mixture in THF, behaving an amphiphilic diblock copolymer in solution state, exhibited a series of morphological transitions from sphere, pearl-necklace-liked rod, worm-liked rod, vesicle, to core−shell-corona aggregates by increasing the OG content. In contrast, the PS-*b*-P4VP/OG mixture in DMF maintained the unimer configuration upon adding OG. Therefore, the complexation-induced morphology of the mixtures of PS-*b*-P4VP and OG can be mediated by adopting different common solvents to affect the self-assembly behavior.

INTRODUCTION

Block copolymers are the focus of the intense research due to their ability to self-assemble into nanostructures with well-defined morphology and size. Many types of block copolymers have been synthesized and their characteristic nano- and micro-phase separation structures have been investigated in solid state and in solution state.[1−11] Micelles are formed that consist of a core containing the insoluble blocks surrounded by a corona of the solvated blocks which exhibit fascinating structures, such as spherical, cylindrical, lamellar, and vesicular micelles, etc.[12,13] In particular, polymeric micelles have received significant attention in drug delivery, templates for the preparation of inorganic nanoparticles including metals, metal oxides or semiconductors, and traps for environmental pollutants or metabolites due to their small size and high stability.[14−19]

It is well-known that the equilibrium aggregate morphologies in solution can be determined by the free-energy balance among three main effects: stretching of the core-forming blocks, inter-coronal interactions, and the interfacial energy between the solvent and the micelle core.[20] Many factors affect the above three terms, and by tuning one of these three factors, the forces balancing the micelles can be upset, leading to a transformation from one morphology into another. Examples of such factors have been investigated previously including the initial copolymer concentration in solution, common solvent used, the amount of selective solvent, block length of the copolymer, and the type and amount of the adding ions (such as salt, acid, or base), etc.[21−23]

Recent advancement has demonstrated that the interpolymer complexation can also lead to micellization through electrostatic interaction[24] or hydrogen bonding.[25] An interpolymer complexation

Received: April 23, 2011
Revised: June 11, 2011
Published: June 17, 2011

can change significantly in terms of the polymers' solublibity and conformation, which facilitates the intercomplex aggregates. Meanwhile, nanostructures can also be obtained involving copolymer and low-molecular-mass compound (LMC, surfactant or organic molecules with a polar head and a nonpolar tail) that have recently been investigated extensively and offer many possibilities to change the microstructure.[25] The micellization behavior of a block copolymer/LMC complex can be controlled by the amount of adding LMC, and a variation in the environment which affect the interaction between block copolymer and LMC.[26] Hydrogen bonds play an important role in the construction of supramolecular polymers by self-assembly due to their moderate bonding energy offering the flexibility for association and dissociation processes.[27] It is well-known that the strength and extent of hydrogen bonding in copolymers or polymer blends depends on their respective affinities between the hydrogen bond donors and acceptors.[11,28−31] In addition, the solvent medium plays other important role to affect or control the type of complex formation. In our previous studies,[30,31] different morphologies used formed from the mixtures of PVPh-*b*-PS and PMMA-*b*-P4VP due to the different chain behaviors of PVPh/P4VP block mixtures in different common solvents. The hydrogen bonding interaction between PS-*b*-PVPh and PMMA-*b*-P4VP in DMF solution is relatively weaker than that in THF solution. As a result, the interpoymer hydrogen-bonded complexation core of PVPh and P4VP chains more stretching, and thus vesicular complexes were formed surrounded by PMMA and PS chains in THF solution. In contrast to the THF solution, DMF solution had relatively lower degree of stretching of the core chains (PVPh/P4VP) and stronger repulsion of the coronal chains (PS and PMMA), consequently, spherical micelles were formed with PVPh/P4VP as the core and PS/PMMA as the corona.

In the present work, we will report that the diverse micellization behaviors can be controlled via introducing octyl gallate (OG) into PS-*b*-P4VP solution in different common solvents (chloroform, DMF, and THF). The solubility of the different common solvents for PS-*b*-P4VP and OG will affect the strength of hydrogen bonding between the P4VP block and OG and the self-assembly behaviors in solution state. As a result, the various micellization behavior can be obtained through using different common solvents.

EXPERIMENTAL SECTION

Materials and Synthesis of Block Copolymer. The styrene monomers (Aldrich, 99%) and 4-vinylpyridine (Aldrich, 99%) were distilled from the finely ground CaH_2 before use. Tetrahydrofuran (THF) as the polymerization solvent for anionic polymerization was purified by distillation under argon from the red solution obtained by diphenylhexyllithium (produced by the reaction of 1,1-diphenylethylene and *n*-BuLi). *sec*-Butyllithium (Acros, 1.3 M in cyclohexane) was used as the initiator for anionic polymerization. Octyl gallate (OG, 99%) was purchased from Fluka, was recrystallized from an ethanol/chloroform (9:1 volume ratio) azeotropic mixture prior to use. Poly(styrene-*block*-4-vinylpyridine) diblock copolymer was synthesized through sequential anionic polymerization as described in the Supporting Information.[32]

Preparation of the PS-*b*-P4VP Aggregates by Adding OG. PS_{61}-*b*-$P4VP_{91}$ and OG with different molar ratio *R* of 4VP/OG (the ratio of OG/4VP is named *R*) ranging from 1/100 to 1 and were dissolved together in chloroform (THF or DMF), and the solutions were stirred for more than 2 days at room temperature. These P4VP blocks are expected to interact with the OG through complementally hydrogen bonding interaction. Scheme 1 presents the hydrogen bonding interaction between P4VP block and OG. All initial copolymer concentrations were maintained at 1 mg/2 mL.

Scheme 1. Schematic Representation of the Interaction that Exists Between P4VP Blocks and Octyl Gallate

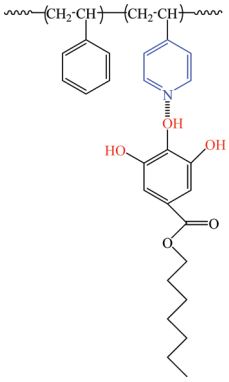

Characterization Methodology. ^1H and ^{13}C NMR spectra were obtained using an INOVA 500 instrument. The molecular weights and PS/P4VP ratios of the various copolymers were evaluated from ^1H NMR spectra and compared with the corresponding values obtained from GPC analysis. Infrared spectra were recorded at 25 °C at a resolution of 1 cm^{-1} on a Nicolet AVATAR 320 FTIR spectrometer using polymer films cast onto KBr pellets from solutions. All FTIR spectra were obtained within the range 4000−400 cm^{-1}; 32 scans were collected at a resolution of 1 cm^{-1} purged with nitrogen to maintain the film's dryness. The hydrodynamic diameters of the assemblies were measured by DLS using a Brookheaven 90 plus model equipment (Brookheaven Instruments Corporation, USA) with a He−Ne laser with a power of 35 mWat 632.8 nm. All DLS measurements were carried out with a wavelength of 632.8 nm at 25 °C with 90° angle of detection. All samples were measured five times. In transmission electron microscopy (TEM) studies, a drop of the micelle solution was sprayed onto a Cu TEM grid covered with a Formvar support film that had been precoated with a thin film of carbon. After 1 min, the excess of the solution was blotted away using a strip of filter paper. All samples were left to dry at room temperature for 1 day prior to observation. After drying, the samples were stained with RuO_4 and viewed under a Hitachi H-7500 TEM instrument operated with an accelerating voltage of 100 kV. The contact angle of the polymer sample was measured at 25 °C using a Krüss GH-100 goniometry interfaced with image-capture software by injecting a 5 μL liquid drop.

RESULTS AND DISCUSSION

Synthesis of Poly(styrene-*block*-4-vinyl pyridine) Diblock Copolymers. The PS-*b*-P4VP diblock copolymer with molecular weight of 15900 $g\cdot mol^{-1}$ and narrow molecular weight distribution (PDI = 1.12) was prepared through anionic living polymerization. ^1H and ^{13}C NMR spectra were recorded for PS-*b*-P4VP sample to confirm its chemical composition and structure. Figure 1a displays typical ^1H NMR spectrum of the diblock copolymer with assignments of its characteristic peaks. The signals due to the aromatic protons and the pyridine ring were observed at 6.1−6.9 ppm and 8.2−8.5 ppm, respectively. Figure 1b displays the ^{13}C NMR spectra of the PS-*b*-P4VP copolymer where the signals corresponding to the aromatic carbons and the pyridine ring were observed at 120−130 ppm and 150 ppm, respectively. Thus, we confirmed that the PS-*b*-P4VP diblock

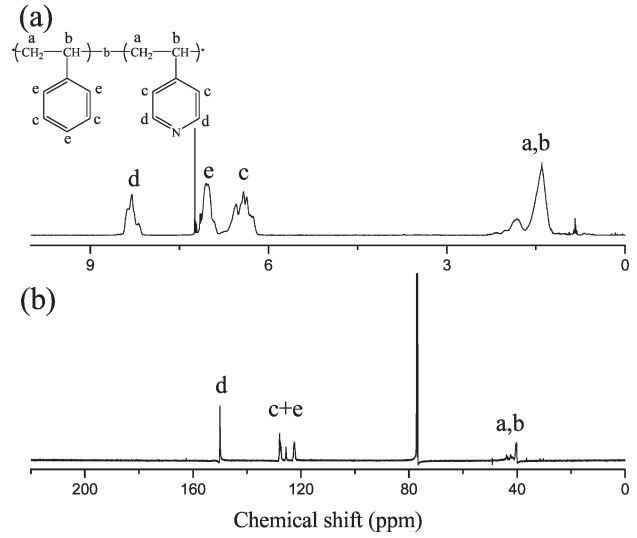

Figure 1. (a) ^{1}H and (b) ^{13}C NMR spectra of PS-*b*-P4VP.

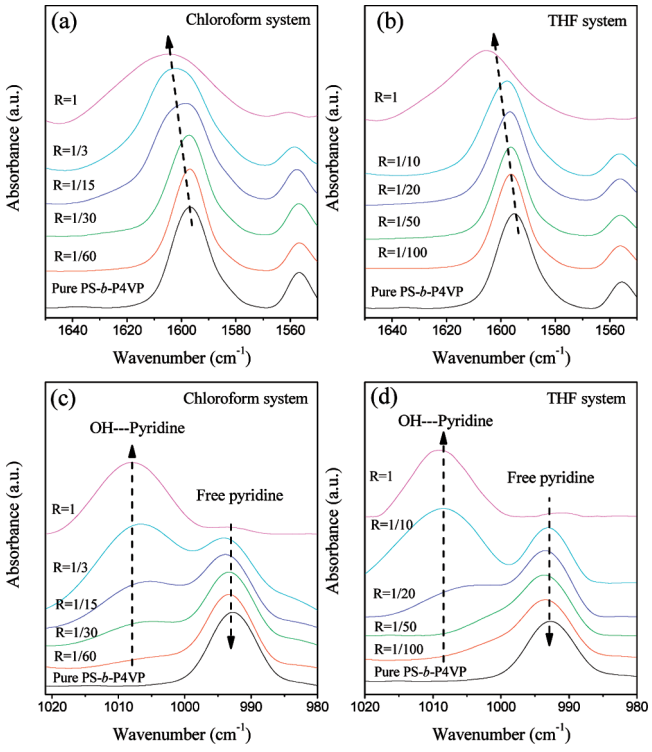

Figure 2. FTIR spectra of the pyridine band of the pure PS-*b*-P4VP and mixtures of OG and PS-*b*-P4VP in the range 1550−1650 cm^{-1} in (a) chloroform and (b) THF and in the range 990−1020 cm^{-1} in (c) chloroform and (d) THF with the different molar ratios, respectively.

copolymer was successfully synthesized through the anionic living polymerization.

FTIR Analyses. Figure 2a,b presents the stretching band of the pyridine groups (1580−1640 cm^{-1}) of the pure PS-*b*-P4VP and the mixtures of PS-*b*-P4VP and OG with various molar ratios cast from THF and chloroform solutions at room temperature. The pyridine band at 1597 cm^{-1} shifted to higher wavenumbers upon adding the OG, indicating that the hydrogen bonding between the pyridine groups of the P4VP blocks and the OH groups of the OG was formed.[33] Furthermore, Figure 2c,d shows the IR spectra of the pyridine ring absorption region (980−1020 cm^{-1}) of the pure PS-*b*-P4VP and the mixtures of PS-*b*-P4VP and OG with various molar ratios cast from THF and chloroform solutions at room temperature. Pure PS-*b*-P4VP has a characteristic band at 993 cm^{-1}, corresponding to the uncomplexed pyridine ring absorption. The new board band at 1005−1010 cm^{-1} is assigned to hydrogen-bonded pyridine units, and its intensity increases upon the increase OG content in comparison to the PS-*b*-P4VP copolymer.[33] As a result, we can confirm that the complex of the OG and P4VP segment are indeed formed due to the stronger hydrogen-bonding interaction between the hydroxyl groups of the OG and pyridine groups of P4VP.

Characterization of the PS-*b*-P4VP/OG Aggregates in Chloroform. The copolymer mixtures were analyzed by dynamic light scattering (DLS). The experimental correlation function was analyzed by the method of the Cumulant and by the CONTIN algorithm, as reported elsewhere.[2] The Stokes−Einstein approximation was used to convert the diffusion coefficient into the hydrodynamic diameter (D_h). Figures 3 and 4 present the hydrodynamic diameters and light scattering intensities of the pure PS-*b*-P4VP and mixtures of the PS-*b*-P4VP and the OG with various molar ratios (R) at a given constant concentration in chloroform. The copolymer without containing OG (Figure 3a) was dissolved in chloroform molecularly as unimer, with D_h of around 8−12 nm and very low scattering intensity. The addition of the OG resulted in D_h increase at R < 1/10 due to binding between polymer and OG which has also been observed for various other blend systems.[34] Figure 3b,c shows that the hydrodynamic diameter distributions for mixtures of PS-*b*-P4VP and OG at R < 1/10 in chloroform are bimodal at 8−12 nm and 120−265 nm. As the R is less than 1/10, the content of the OG is lower in system, the free unbound polymer chains and those bound with OG in solution coexisted. The interaction between PS-*b*-P4VP and OG leads to the formation of aggregates composed of the P4VP/OG-complex core and PS-corona in the system because the solubility of the bound polymer chains becomes relatively lower. As a result, the bimodal distributions corresponding to free unbound polymer chains (8−12 nm) and aggregates of the OG bound polymers are formed. However, the scattering intensity was low even though the aggregates were formed in the system at R < 1/10, implying that the structures of these aggregates were loose and unstable. As the OG content was low, the loose and giant aggregates (i.e., big micelles) were formed because the amount of the P4VP blocks binding to OG was low and cannot provide the sufficient driving force to assemble the dense and stable micelle structure. With further increasing the OG content, the D_h decreased remarkably to 40 nm. While the scattering intensity was sharply increased, and the aggregates showed a remarkably narrow size distribution. This result indicates that these aggregates became denser with a well-defined structure, as a result of the formation of micellization. The insolubility of the bound pyridine units due to enough bound pyridine groups drives the aggregation of the P4VP/OG complex to form the micellization with further increase in OG content. ^{1}H spectra data provided further evidence to demonstrate the formation of complexation between the P4VP blocks and OG. Figure 5 presents the ^{1}H NMR spectra of the pure PS-*b*-P4VP and mixtures of the PS-*b*-P4VP and OG with the different R in $CDCl_3$. The intensity of the signals due to H_d of P4VP at 8.2−8.5 ppm was depressed at R = 1/20, finally, it totally disappeared at R = 1. Additionally, at R = 1, the intensity ratio

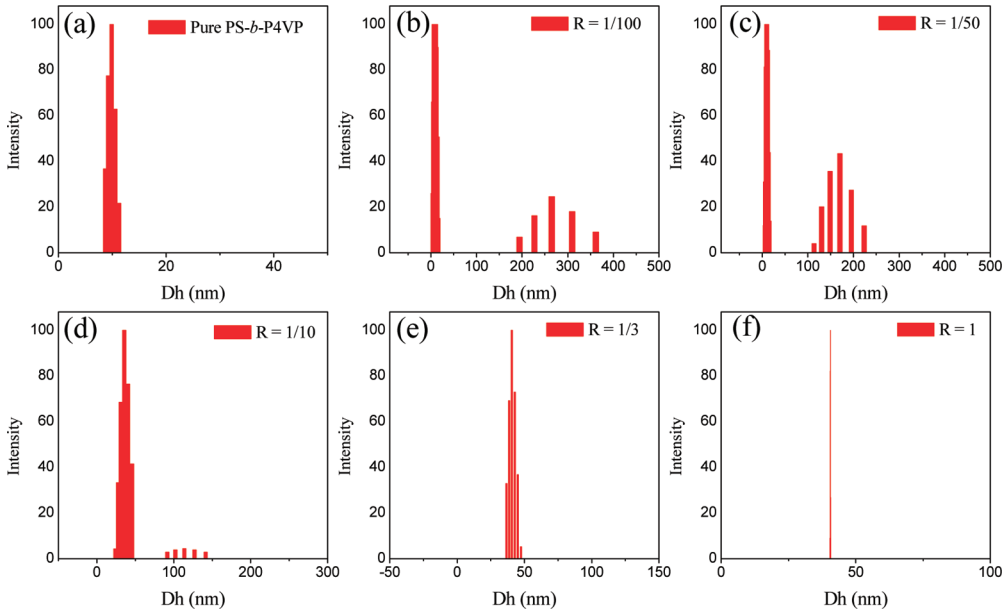

Figure 3. The hydrodynamic diameter distribution of the mixtures of OG and PS-*b*-P4VP with the different molar ratios in chloroform.

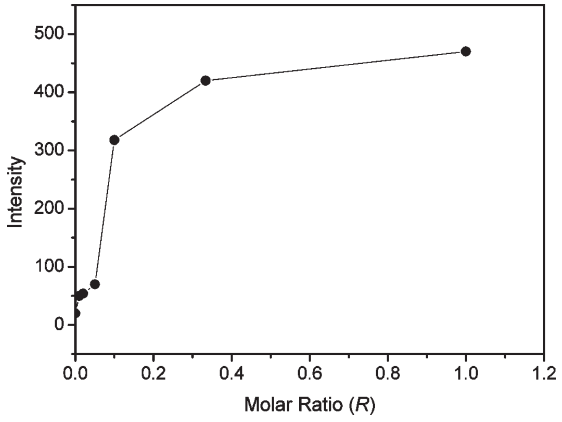

Figure 4. The intensity of the scattering of the mixtures of OG and PS-*b*-P4VP with the different molar ratios in chloroform.

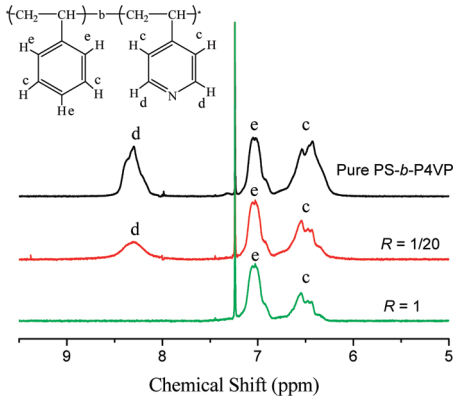

Figure 5. ^{1}H NMR spectra of the (a) pure PS-b-P4VP and the mixtures of OG and PS-*b*-P4VP (b) at R = 1/20 and (c) R = 1 in $CDCl_3$.

of H_e to H_c comes close to 3/2, corresponding to the number ratio of the H_e to H_c in the benzene rings. These ^{1}H spectra data indicate that the formation of aggregates between the bound P4VP blocks caused depression or even disappearance of P4VP signals because the mobility was restricted.

The morphologies of these noncovalent complex aggregates were investigated by transmission electron microscopy (TEM). Figure 6 presents the TEM images for mixtures of the PS-*b*-P4VP and OG with different molar ratios R from chloroform solutions. At R = 1/50, the aggregates possess diameter about 300 nm and weak contrast, indicating that the structure of these aggregates were loose and polydisperse. As the R was increased to 1/10, the aggregates showed dual size distribution, one has a diameter about 200 nm, and another possesses a diameter about 50 nm. The former aggregates correspond to the loose structure, whereas the latter arose from the dense micelles due to enough bound pyridine units. When the R was increased to 1/3 and 1, these structures showed uniform size and well-defined shape spheres. These TEM images are consistent with the DLS results, implying that the complexation-induced micellization by hydrogen-bonding indeed occurred.

Figure 7 shows various SEM images of cast films for mixtures of PS-*b*-P4VP and OG with different molar R in chloroform solution after solvent evaporation. No morphology was observed from the PS-*b*-P4VP without containing OG from chloroform solution as shown in Figure 7a. Most interestingly, the honeycomb-structured porous films were obtained by adding the OG. At R = 1/100, the broken and imperfect porous film was obtained. With increasing the OG content to R = 1/50, only irregular pores were formed. Further increasing the molar ratio R from 1/50 to 1/10, 1/3, and 1, the degree of the regularity of the porous film increased remarkably, and the pore size decreased. Additionally, Fast Fourier transfer (FFT) pattern (Figure 7, inset images) also indicated a hexagonal arrangement of the pores was formed on the surface, while the regularity of the porous film increased upon increasing the OG content. By casting onto solid substrates, these aggregates spontaneously converted into honeycomb structure. The spherical shape of the porous structure reflected the shape of template water droplets and the observed honeycomb architecture was formed by the "breath figures" method.[35−40] According

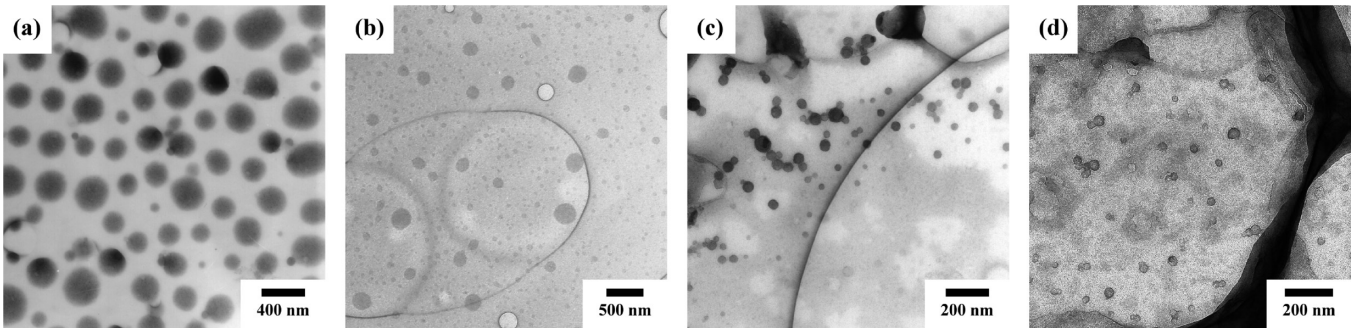

Figure 6. TEM images of the morphologies of the mixtures of OG and PS-*b*-P4VP (a) at R = 1/50, (b) at R = 1/10, (c) at R = 1/3, and (d) at R = 1.

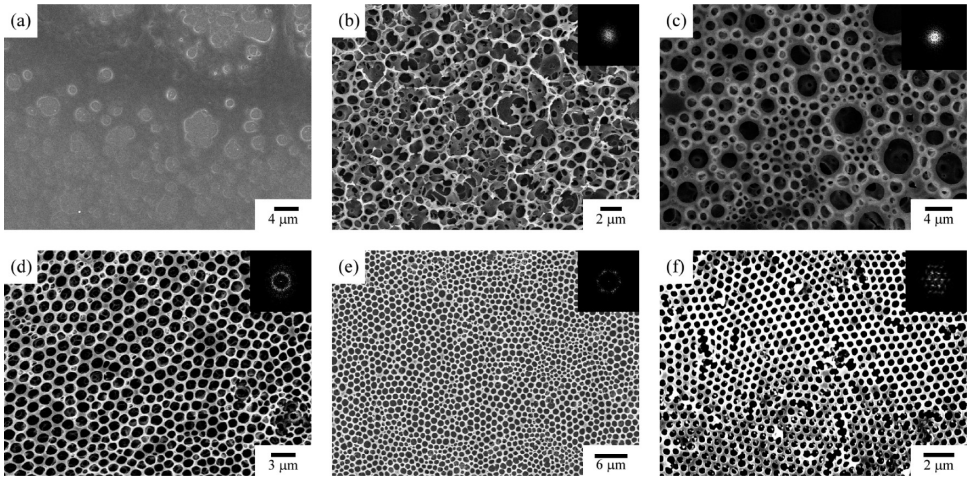

Figure 7. SEM images of the morphologies of the (a) pure PS-*b*-P4VP and the mixtures of OG and PS-*b*-P4VP (b) at R = 1/100, (c) at R = 1/50, (d) at R = 1/10, (e) at R = 1/3, and (f) at R = 1.

to the "breath figures" mechanism, the water droplets act as the template to form the honeycomb structure, and the stabilization of the water droplets is the crucial point for preparing a regular honeycomb structure. The interfacial activity of the various aggregates of different mixtures provided different degrees of the stabilization of the water droplets and resulted in the different structures. It is well-known that the ability of adsorbed aggregates to stabilize the water-solution interface is relative to the aggregates wettability. The wettability of the aggregates at the solvent−water interface can be quantified by the corresponding interfacial contact angle θ_{ws}, which can be calculated according to the modified Young's equation:[41]

$$\theta_{ws} = \cos^{-1}\left[\frac{(\gamma_w \cos\theta_w - \gamma_s \cos\theta_s)}{\gamma_{w/s}}\right] \quad (1)$$

where γ_w and γ_s are the surface tensions of water and solution, respectively, $\gamma_{w/s}$ is the interfacial tension between water and solution, and the static contact angles of water and chloroform (θ_w and θ_s) can be measured on the flat film of nanoparticles, respectively. If the particles are either too hydrophilic or too hydrophobic, then they tend to remain dispersed in either the aqueous ($\theta_{ws} < 90°$) or the oil phase ($\theta_{ws} > 90°$) and cannot sufficiently stabilize the water droplets. The wettability of the aggregates is believed to play an important role for forming a honeycomb structure.

Table 1. Summary of the Structural Parameters and Corresponding θ_w and θ_{ws} of Aggregates Formed by PS-*b*-P4VP/OG Mixtures in Chloroform

molar ratio, R	morphology	θ_w (deg) ± 1°	θ_{ws} (deg) ± 1°
1/100	loose aggregate	105	N/A[a]
1/50	loose aggregate	102	N/A[a]
1/10	loose aggregate + spherical micelle	89	143
1/3	spherical micelle	73	100
1	spherical micelle	70	94

[a] It cannot be calculated according to eq 1

The wettability of the aggregate with the different molar ratio R at the water-solvent interface could be quantified by the corresponding contact angles, and the θ_{ws} can be calculated according to eq 1 by measuring the contact angles on the flat films.[42−49] We measured the θ_w and estimated θ_s 2252 0 for chloroform entirely wets all film surfaces of these aggregates. The θ_w and the corresponding calculated contact angles θ_{ws} at the interface between water and chloroform are summarized in Table 1. The θ_w gradually decreased from 105 to 70° upon increasing R from 1/100 to 1. The θ_{ws} values cannot be obtained at R = 1/100 and 1/50, implying that most molecularly dispersed PS-*b*-P4VP/OG complexes and the loose aggregates tended to disperse in the

chloroform phased due to the high hydrophobicity and cannot stay at the water/chloroform interface for stabilizing the water droplets. As expected, the irregular porous films with a relatively broad distribution of the pore size were induced because of the fusion of the water droplets. With further increasing R to 1/10, 1/3, and 1, the θ_{ws} progressively decreased to close 90°, reflecting that the hydrophobicity of the aggregates decreased as the loose aggregates became the dense micelles, and these micelles effectively stabilized the water droplets and preserved the structure of the porous film during drying. Then, an order honeycomb was obtained as shown in Figure 7f. As a result, the dense and monodisperse micelles have a suitable wettability to stabilize the water droplets to prevent the condensation of water droplets; however, the loose structure contained a lot of solvent and became too hydrophobic to stabilize the water droplets. In summary, the mixtures with the different R can self-assemble the different aggregates which possess the different wettability and provide the porous films with the variou regularity.

Characterization of the PS-*b*-P4VP/OG Aggregates in THF and DMF. Now, we turn our attention to the behaviors of the mixtures of the PS-*b*-P4VP and OG with the different R in THF solutions. Figure 8 presents the ^{1}H NMR spectra of the pure PS-*b*-P4VP and mixtures of the PS-*b*-P4VP and OG with the different R in THF-*d*. The unusual phenomenon was obtained that the intensity of signals due to H_d of P4VP at 8.2−8.5 ppm increased with increasing the OG content, and the intensities of the signals due to H_c and H_e were depressed. These results indicated that the P4VP blocks had the reverse behavior and became more mobile by adding OG. Thus, the core-domains composed of P4VP and bound P4VP blocks were swollen and increased the mobility.

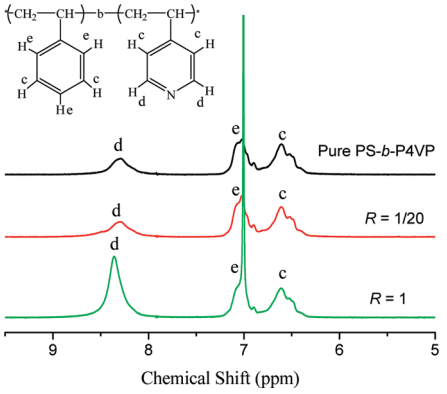

Figure 8. ^{1}H NMR spectra of the (a) pure PS-*b*-P4VP and the mixtures of OG and PS-*b*-P4VP (b) at R = 1/20 and (c) R = 1 in THF-*d*.

Figure 9 presents the hydrodynamic diameters of the pure PS-*b*-P4VP and mixtures of the PS-*b*-P4VP and the OG with various molar ratios (R) at a given constant concentration in THF. The aggregates with an average diameter of the range 35−40 nm were observed at R < 1/50. As increasing the OG content, the aggregate size increased to 74 nm at R = 1/20, 120 nm at R = 1/10, 240 nm at R = 1/5, and 230 nm at R = 1, implying that the bound PS-b-P4VP with OG would change their structures of the assembled objects. However, it is difficult to predict that this increase in the hydrodynamic diameter of the objects is caused by the swell of aggregates or the change of aggregates to other morphologies. In order to clarify the cause of the changes in the hydrodynamic diameter, we will explore the TEM images of this system. Figure 10 shows the TEM images for various morphologies formed from the mixtures of the PS-*b*-P4VP and OG with different R in THF. Nanospherical micelles of the PS-*b*-P4VP without OG were formed as shown in Figure 9a, implying that the THF has the different selectivity for the PS and P4VP block (i.e., the THF has a better solubility for the PS blocks) resulting in the formation of the micelles. At R = 1/50, the morphology of the mixture maintained the spherical micelle. At R = 1/20, the aggregates transformed into coexisting pearl-necklace-liked rod micelles and spherical micelles as shown in Figure 10c. On further increasing the OG content, the morphology of the aggregates changed to the worm-liked micelles at R = 1/10, then to the vesicular aggregates at R = 1/5. Most interestingly, at R = 1, the morphology of the aggregates transferred to an unusual structure which was similar to the core−shell−corona structure as shown

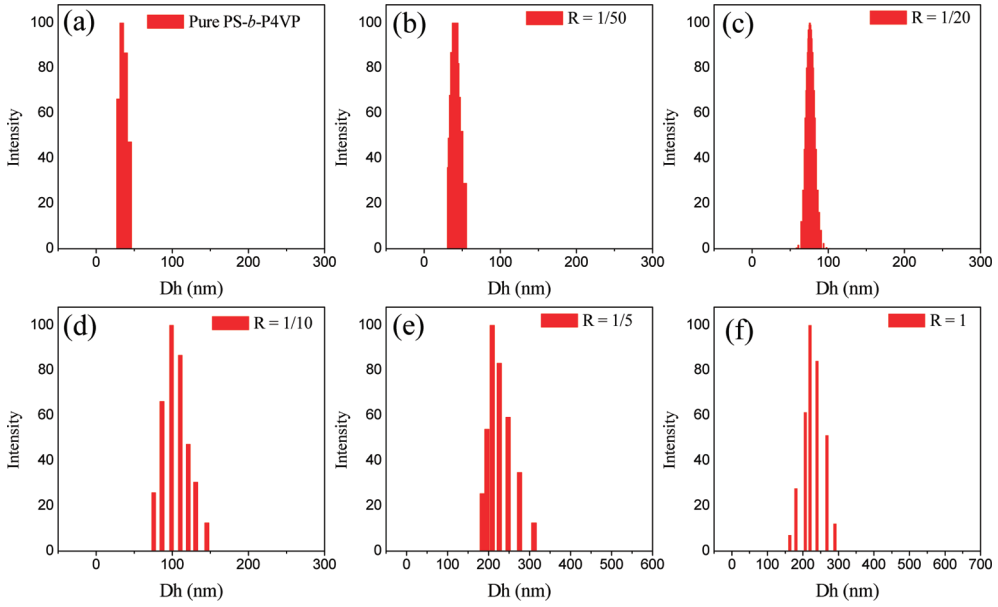

Figure 9. The hydrodynamic diameter distribution of the mixtures of OG and PS-*b*-P4VP with the different molar ratios in THF.

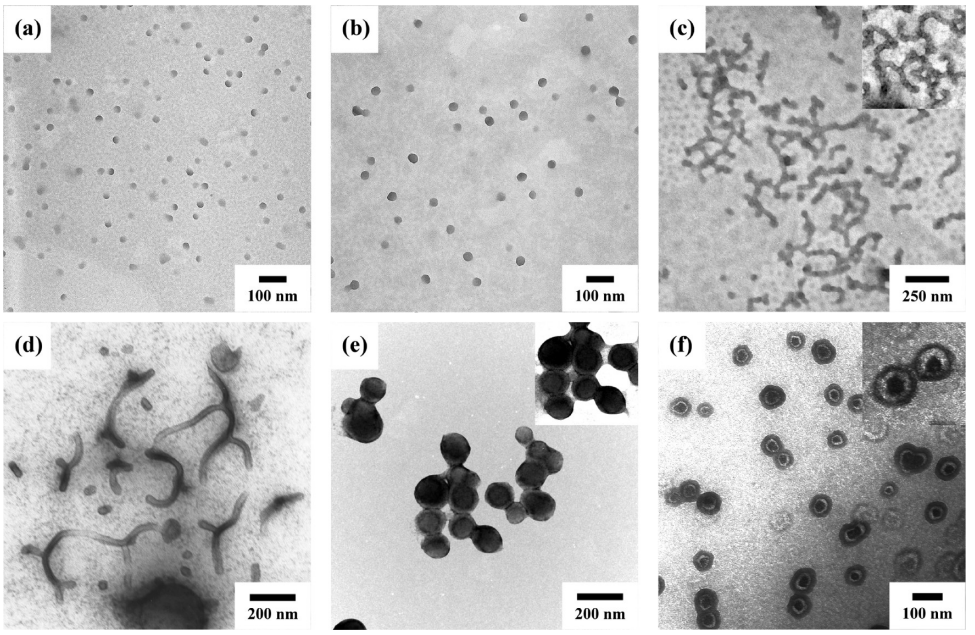

Figure 10. TEM images of the morphologies of the (a) pure PS-*b*-P4VP and the mixtures of OG and PS-*b*-P4VP (b) at $R = 1/50$, (c) at $R = 1/20$, (d) at $R = 1/10$, (e) at $R = 1/5$, and (f) at $R = 1$.

in Figure 10f. It is well-known that several factors influence the morphologies of block copolymer aggregates in a solution;[21,32,50] the free energies of aggregation are affected by the intercoronal chain interaction, the core−coronal interfacial energy, and the degree of core-chain stretching. Here, the OG moieties were capable of forming strong hydrogen-bonding interaction with P4VP blocks. On the asis of the NMR analysis, the OG could increase the size of the core and promote the architectural changes. In addition, it is believed that the long tail of OG could reduce the intercoronal chain interaction by providing the more space between the corona chains due to their hydrophobic character. The degree of P4VP stretching increases in response to the increase in the core diameter. This increased chain stretching is subject to an entropic penalty, and in the present system the aggregates undergo morphological change in order to relieve this entropy strain. At $R = 1$, the core−shell-corona like aggregate was observed. When the added OG was higher, the excess of the OG would accumulate the inner domain (i.e., P4VP/OG complex phase) of the vesicle and expand domain size. Meanwhile, the gray thin layer of the inner domain was obtained as shown in Figure 10f, because the electronic density of OG is lower. Thus, we speculated that the vesicle transferred to the core−shell-corona like aggregate, and the core, shell, and corona were composed of PS, P4VP/OG complex, and PS, respectively. Consequently, the addition of OG can induce a series of morphological transition from sphere, pearl-necklace-liked rod, worm-liked rod, vesicle, to core−shell−corona aggregates, indicating that the morphologies can be controlled by changing the OG content. Meanwhile, the mixtures of the PS-*b*-P4VP and OG with the different R in DMF solutions were studied. Figure 11 displays the hydrodynamic diameter and light scattering intensities of the mixtures of the PS-*b*-P4VP and OG with the different R in DMF. The D_h maintained the similar value upon adding the OG and even at $R = 1$, and the intensity was weak, indicating that the addition of the OG cannot lead any self-assembled aggregates in DMF. Taft et al. demonstrated that the solvatochromic comparison method was used to unravel, quantify, correlate, and rationalize multiple solvent effects on many types of physicochemical properties and presented reactivity parameters, and comprehensive collection of π^*, α, and β values.[51,52] The π^* scale is an index of solvent dipolarity/polarizability, which was measured the ability of the solvent to stabilize a change or a dipole by virtue of its dielectric effect. The α scale of solvent HBD (hydrogen-bond donor) acidities describes the ability of the solvent to donate a proton in a solvent-to-solute hydrogen bond. The β scale of HBA (hydrogen-bond acceptor) basicities provides a measure of the solvent's ability to accept a proton (donate an electron pair) in a solute-to-solvent hydrogen bond. Due to Taft's reports,[51,52] the values of β of chloroform, THF, and DMF are 0.00, 0.55, and 0.69, respectively, and the values of π^* of chloroform, THF, and DMF are 0.58, 0.58, and 0.88. The values of β and π^* indicate that chloroform and THF is less polar than DMF, and DMF has higher hydrogen-bond-acceptor ability than chloroform and THF. Thus, we speculated that the hydrogen-bonding between the P4VP blocks and OG were not efficiently formed due to the polarity of DMF, resulting that the mixtures of the PS-*b*-P4VP and OG cannot form aggregates. In addition, the hydrogen bonding interaction between OG and P4VP block also could be found by FTIR analyses (for brevity not shown here).

In summary, Figure 12 displays our proposed mechanism for the morphologies of the mixtures of the PS-*b*-P4VP and OG from the different solvent. For chloroform system, the self-assembled nano-objects were formed by adding OG, and the honeycomb structures were obtained through these aggregates acting as the stabilizer for the water droplets. For THF system, a series of morphological transition was induced to reduce the free energy of the system. For the DMF system, the unimer-to-micelle transition cannot be lead through adding OG due to the relatively weak hydrogen-bonding interaction in DMF. As a result, the complexation-induced morphologies of the mixtures of PS-*b*-P4VP and OG can be mediated by adopting different solvents to affect the self-assembly behavior.

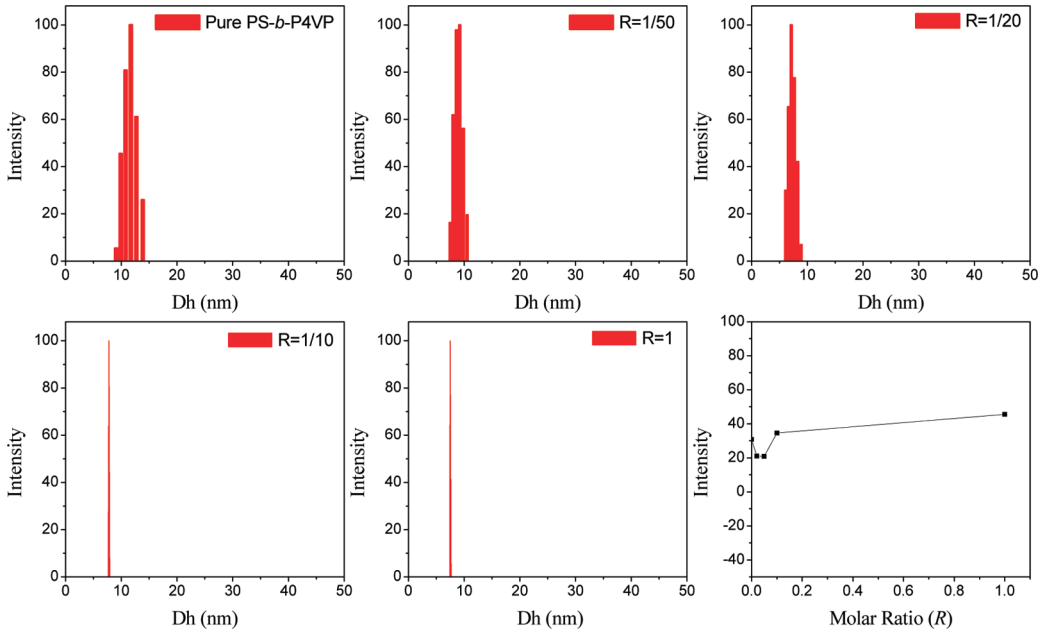

Figure 11. The hydrodynamic diameter distribution and intensities of the mixtures of OG and PS-*b*-P4VP with the different molar ratios in DMF.

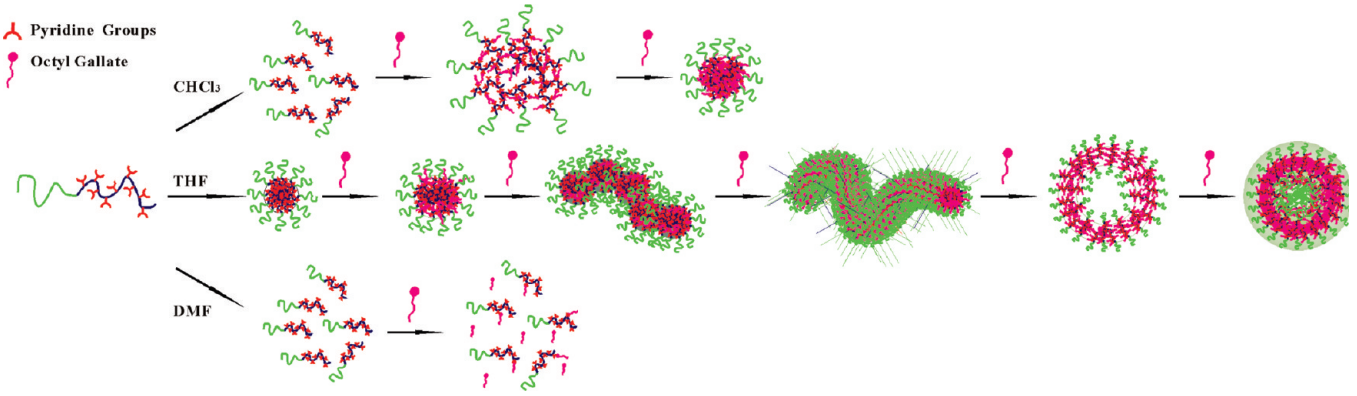

Figure 12. Proposed the aggregate behaviors of the mixtures of OG and PS-*b*-P4VP with the different molar ratios from the different common solvents.

CONCLUSIONS

Hydrogen bonding between P4VP blocks of PS-*b*-P4VP diblock copolymer and OG in different solvents results in various complexation-induced micellization. Both FTIR and NMR analyses provided evidence for the formation of the P4VP binding to OG due to hydrogen bonding between the P4VP blocks and OG. Integrated results of TEM images and DLS data clearly show that the self-assembly behaviors of the mixtures of the PS-*b*-P4VP and OG can be modulated via adopting the different solvents. For PS-*b*-P4VP/OG mixture in chloroform, the morphological transitions were induced from the unimer configuration to swollen aggregate and complex-micelles by adding OG. Interestingly, the complex-micelles can lead the formation of the honeycomb structure from chloroform solution. The PS-*b*-P4VP/OG mixture in THF, behaving an amphiphilic diblock copolymer in solution state, exhibited a series of morphological transitions from sphere, pearl-necklace-liked rod, worm-liked rod, vesicle, to core—shell-corona aggregates by increasing the OG content. In contrast, the PS-*b*-P4VP/OG mixture in DMF maintained the unimer configuration upon adding OG due to relatively weak hydrogen-bonding.

ASSOCIATED CONTENT

Supporting Information. Poly(styrene-*block*-4-vinylpyridine) diblock copolymer synthesis through sequential anionic polymerization. This material is available free of charge via the Internet at http://pubs.acs.org.

AUTHOR INFORMATION

Corresponding Authors

*Tel: 886-3-5131512; Fax: 886-3-5131512; E-mail: changfc@mail.nctu.edu.tw. (F.-C.C.). Tel/Fax: 886-7-5254099; E-mail: kuosw@faculty.nsysu.edu.tw (S.-W.K.).

REFERENCES

(1) Patten, T. E.; Matyjaszewski, K. *Adv. Mater.* **1998**, *10*, 901.
(2) Sakurai, S.; Kawada, H.; Hashimoto, T.; Fetter, L. J. *Macromolecules* **1993**, *26*, 5796.
(3) Hamley, I. W. *The Physics of Block Copolymers*;Oxford University Press: New York, 1998.

(4) Kreutzer, G.; Ternat, C.; Nguyen, T. Q.; Plummer, C. J. G.; Manson, J.-A. E.; Castelletto, V.; Hamley, I. W.; Sun, F.; Sheiko, S. S.; Herrmann, A.; Ouali, L.; Sommer, H.; Fieber, W.; Velazco, M. I.; Klok, H.-A. *Macromolecules* **2006**, *39*, 4507.
(5) Cong, Y.; Li, B.; Han, Y.; Li, Y.; Pan, C. *Macromolecules* **2005**, *38*, 9836.
(6) He, H.; Huang, L.; Liang, H.; Pan, C. *J. Chem. Phys.* **2003**, *118*, 9861.
(7) Hadjichristidis, N.; Iatrou, H.; Pitsikalis, M.; Pispas, S.; Avgeropoulous, A. *Prog. Polym. Sci.* **2005**, *30*, 725.
(8) Khelfallah, N.; Gunari, N.; Fischer, K.; Gkogkas, G.; Hadjichristidis, N.; Schmidt, M. *Macromol. Rapid Commun.* **2005**, *26*, 1693.
(9) Asari, T.; Matsuo, S.; Takano, A.; Matsushita, Y. *Macromolecules* **2005**, *38*, 8811.
(10) Zheng, R.; Liu, G.; Yan, X. *J. Am. Chem. Soc.* **2005**, *127*, 15358.
(11) Chen, S. C.; Kuo, S. W.; Jeng, U S.; Su, C. J.; Chang, F. C. *Macromolecules* **2010**, *43*, 1083.
(12) Rodríguez-Hernández, J.; Chécot, F.; Gnanou, Y.; Lecommandoux, S. *Prog. Polym. Sci.* **2005**, *30*, 691.
(13) Kataoka, K.; Kwon, G. S.; Yokoyama, Y.; Okano, T.; Sakurai, Y. *J. Contolled Release* **1993**, *24*, 119.
(14) Kitazawa, Y.; Miyata; Furukawa, S.; Kataoka, K. *Adv. Mater.* **2004**, *16*, 699.
(15) Yan, X.; Liu, G.; Haeussler, M.; Tang, B. Z. *Chem. Mater.* **2005**, *17*, 6053.
(16) Aizawa, M.; Buriak, J. M. *J. Am. Chem. Soc.* **2005**, *127*, 8932.
(17) Djalali, R.; Li, S.-Y.; Schmidt, M. *Macromolecules* **2002**, *35*, 4282.
(18) Selvan, S. T.; Hayakawa, T.; Nogami, M.; Moller, M. *J. Phys. Chem. B.* **1999**, *103*, 7441.
(19) Wang, X. S.; Wang, H.; Coombs, N.; Winnik, M. A.; Manners, I. *J. Am. Chem. Soc.* **2005**, *127*, 8924.
(20) Zhang, L.; Eisenberg, A. *J. Am. Chem. Soc.* **1996**, *118*, 3168.
(21) Zhang, L.; Shen, H.; Eisenberg, A. *Macromolecules* **1997**, *30*, 1001.
(22) (a) Harada, A.; Kataoka, K. *Macromolecules* **1995**, *28*, 5294. (b) Alexander, V.; Kabanov, A. V.; Bronich, T. K.; Kabanov, V. A.; Yu, K.; Eisenberg, A. *Macromolecules* **1996**, *29*, 6797.
(23) (a) Duan, H.; Chen, D.; Jiang, M.; Gan, W.; Li, S.; Wang, M.; Gong, J. *J. Am. Chem. Soc.* **2001**, *123*, 12097. (b) Yao, X.; Chen, D.; Jiang, M. *Macromolecules* **2004**, *37*, 4211. (c) Zhu, J.; Yu, H.; Jiang, W. *Macromolecules* **2005**, *38*, 7492.
(24) Ruokolainen, J.; Saariaho, M.; Ikkala, O.; ten Brinke, G.; Thomas, E. L.; Torkkeli, M.; Serimaa, R. *Macromolecules* **1999**, *32*, 1152.
(25) (a) Ruokolainen, J.; Mäkinen, R.; Torkkeli, M.; Makela, T.; Serimaa, R.; ten Brinke, G.; Ikkala, O. *Science* **1998**, *280*, 557. (b) Ruokolainen, J.; ten Brinke, G.; Ikkala, O. *Adv. Mater.* **1999**, *11*, 777. (c) Ruokolainen, J.; Torkkeli, M.; Serimaa, R.; Komanschek, E.; ten Brinke, G.; Ikkala, O. *Macromolecules* **1997**, *30*, 2002. (d) de Moel, K.; Alberda van Ekenstein, G. O. R.; Nijland, H.; Polushkin, E.; ten Brinke, G.; Maki-Ontto, R.; Ikkala, O. *Chem. Mater.* **2001**, *13*, 4580.
(26) (a) Wang, M.; Jiang, M.; Ning, F.; Chen, D.; Liu, S.; Duan, H. *Macromolecules* **2002**, *35*, 5980. (b) Liu, S.; Zhu, H.; Zhao, H.; Jiang, M.; Wu, C. *Langmuir* **2000**, *16*, 3712.
(27) Kuo, S. W.; Chang, F. C. *Macromolecules* **2001**, *34*, 4089.
(28) Kuo, S. W.; Chang, F. C. *Macromolecules* **2001**, *34*, 5224.
(29) He, Y.; Zhu, B.; Inoue, Y. *Prog. Polym. Sci.* **2004**, *29*, 1021.
(30) Kuo, S. W.; Tung, P. H.; Lai, C. L.; Jeong, K. U.; Chang, F. C. *Macromol. Rapid Commun.* **2008**, *29*, 229.
(31) Hsu, C. H.; Kuo, S. W.; Chen, J. K.; Ko, F. H.; Liao, C. S.; Chang, F. C. *Langmuir* **2008**, *24*, 7727.
(32) Chen, S. C.; Kuo, S. W.; Liao, C. S.; Chang, F. C. *Macromolecules* **2008**, *41*, 8865.
(33) Ruokolainen, J.; Torkkeli, M.; Serimaa, R.; Vahvaselka, S.; Saariaho, M.; ten Brinke, G.; Ikkala, O. *Macromolecules* **1996**, *29*, 6621.
(34) Tan, J. F.; Too, H. P.; Hatton, T. A.; Tam, K. C. *Langmuir* **2006**, *22*, 3744.
(35) Widawski, G.; Rawiso, M.; Francois, B. *Nature* **1994**, *369*, 387.
(36) Limaye, A. V.; Narhe, R. D.; Dhote, A. M.; Ogale, S. B. *Phys. Rev. Lett.* **1996**, *76*, 3762.
(37) Maruyama, N.; Koito, T.; Nishida, J.; Sawadaishi, T.; Cieren, X.; Ijiro, K.; Karthaus, O.; Shimomura, M. *Thin Solid Films* **1998**, *327*–*329*, 854.
(38) Srinivasarao, M.; Collings, D.; Philips, A.; Patel, S. *Science* **2001**, *292*, 79.
(39) Stowell, C.; Korgel, B. A. *Nano Lett.* **2001**, *1*, 595.
(40) Nishikawa, T.; Ookura, R.; Nishida, J.; Arai, K.; Hayashi, J.; Kurono, N.; Sawadaishi, T.; Hara, M.; Shimomura, M. *Langmuir* **2002**, *18*, 5734.
(41) Shah, P. S.; Sigman, M. B., Jr.; Stowell, C. A.; Lim, K. T.; Johnston, K. P.; Korgel, B. A. *Adv. Mater.* **2003**, *15*, 971.
(42) Park, M. S.; Kim, J. K. *Langmuir* **2004**, *20*, 5347.
(43) Cheng, C. X.; Tian, Y.; Shi, Y. Q.; Tang, R. P.; F. Xi, F. *Langmuir* **2005**, *21*, 6576.
(44) Lin, C. L.; Tung, P. H.; Chang, F. C. *Polymer* **2005**, *46*, 9304.
(45) Li, J.; Peng, J.; Huang, W.; Wu, Y.; Fu, J.; Cong, Y.; Xue, L.; Han, Y. *Langmuir* **2005**, *21*, 2017.
(46) Park, M. S.; Joo, W.; Kim, J. K. *Langmuir* **2006**, *22*, 4594.
(47) Sun, H.; Li, H.; Bu, W.; Xu, M.; Wu, L. *J. Phys. Chem. B* **2006**, *110*, 24847.
(48) Tung, P. H.; Kuo, S. W.; Jeong, K. U.; Cheng, S. Z. D.; Huang, C. F.; Chang, F. C. *Macromol. Rapid Commun.* **2007**, *28*, 271.
(49) Kadla, J. F.; Asfour, F. H.; Bar-Nir, B. *Biomacromolecules* **2007**, *8*, 161.
(50) Tung, P. H.; Kuo, S. W.; Chen, S. C.; Lin, C. L.; Chang, F. C. *Polymer* **2007**, *48*, 3192.
(51) Kamlet, M. J.; Taft, R. W. *J. Am. Chem. Soc.* **1976**, *98*, 377.
(52) Kamlet, M. J.; Abboud, J. L. M.; Abraham, M. H.; Taft, R. W. *J. Org. Chem.* **1983**, *48*, 2877.